JOURNAL OF GEOPHYSICAL RESEARCH, VOL. 90, NO. A2, PAGES 1531–1541, FEBRUARY 1, 1985

Lightning-Induced Electron Precipitation from the Magnetosphere

H. C. CHANG[1] AND U. S. INAN

Space, Telecommunications and Radioscience Laboratory, Stanford University, California

Precipitation of radiation belt particles induced by whistlers that are generated by atmospheric lightning discharges and propagate over L shells of 2–4.5 is considered. Using a test particle model of the whistler-particle interaction, the energy spectra and temporal profile of whistler-induced fluxes as a function of L shell are quantitatively determined for a representative plasmaspheric cold plasma distribution. Results indicate that for higher energy electron precipitation ($E > 40$ keV) there exists an inner magnetospheric region ($2 < L < 3$) where the level of whistler-induced precipitation can be expected to be comparatively high. Implications of this finding in terms of observational results are discussed.

1. INTRODUCTION

Wave-induced precipitation of radiation belt electrons and the associated ionospheric effects have attracted much attention in recent years. In this paper, we discuss such precipitation caused by whistlers that are generated by atmospheric lightning discharges and that propagate in the magnetosphere in field-aligned "ducts" of enhanced ionization [*Helliwell*, 1965].

Precipitation induced by whistler mode VLF waves has been recognized as an important loss process for radiation belt electrons on closed magnetic field lines at subauroral latitudes [*Lyons et al.*, 1972]. The possible role in this precipitation of lightning-generated whistlers was suggested two decades ago [*Dungey*, 1963; *Cornwall*, 1964]. Since then, this question has received increasing attention as a result of experimental evidence suggesting a one-to-one association between whistlers (or emissions triggered by them) and ionospheric effects of precipitation [*Rosenberg et al.*, 1971; *Rycroft*, 1973; *Helliwell et al.*, 1973, 1980; *Carpenter and LaBelle*, 1982; *Doolittle and Carpenter*, 1983].

A particular related phenomenon of interest is the so-called "Trimpi" effect, involving perturbations of the amplitude and/or phase of subionospheric VLF/LF signals due to whistler-induced precipitation. This phenomenon was first reported by *Helliwell et al.* [1973]; correlations were observed between ground-observed whistlers and perturbations in the wave intensity of fixed frequency VLF navigational signals propagating in the nighttime earth-ionosphere waveguide. The perturbations were attributed to aberrations in the earth-ionosphere waveguide mode structure caused by localized transient enhancements of the electron population in the ionospheric D region produced by energetic (> 40 keV) electrons precipitated by the whistlers.

Recent studies of these events at Palmer Station, Antarctica (65°S, 64°W, $L \simeq 2.3$) have shown that events occur more commonly than previously believed [*Leyser et al.*, 1984], that perturbations can be seen on signals with frequencies as high as 800 kHz [*Carpenter et al.*, 1984], and that the whistler induced precipitation can in many cases occur on L-shells as low as L=2 [*Carpenter and LaBelle*, 1982]. Thus far the "Trimpi" effect is the only ground-based technique by which wave-induced burst precipitation has been regularly detected within the dense plasmasphere. When observed outside the plasmasphere, such events are commonly associated with emissions triggered by whistlers, while events occurring within the inner plasmasphere usually represent precipitation by the whistler itself, with no apparent associated triggering of emissions.

In a recent study using a particle detector on the low-altitude S81-1 satellite, bursts of precipitating electrons were observed in one-to-one association with lightning generated whistlers recorded at a ground station [*Voss et al.*, 1984], thus supporting and extending the inferences based on ground-based observations.

The recent experimental results bring to fore the questions about the possible role of lightning and thunderstorms as a loss mechanism for radiation belt electrons and thus about their possible importance in the coupling of the troposphere to the ionosphere and the magnetosphere. The experiments show direct evidence of the removal of electrons from the radiation belts in single events, but the overall effects of whistler-induced precipitation are not known.

As a first step toward numerical modeling of such overall effects, we present here quantitative estimates of the precipitation induced by individual whistlers as a function of L over the range L=2–4.5. Theoretical modeling of the magnetospheric interactions of energetic particles with whistler waves having slowly varying frequency was recently developed. In this paper, we employ a test particle model [*Inan et al.*, 1982; *Chang et al.*, 1983] to determine the time evolution and energy spectra of the precipitated energy fluxes induced by lightning-generated whistler wave pulses propagating along the earth's magnetic field lines. This model takes into account the full nonlinear wave-induced pitch angle scattering, including relativistic energies as well as the effects of changing frequency and dispersion within a variable-frequency wave packet. The model is used to compute the pitch angle scattering of a large number of individual test particles in order to infer the perturbations of the electron

[1] Now at Department of Electrical Engineering, National Taiwan University, Taipei, Republic of China

Paper number 4A8265.
0148-0227/85/004A-8265$05.00

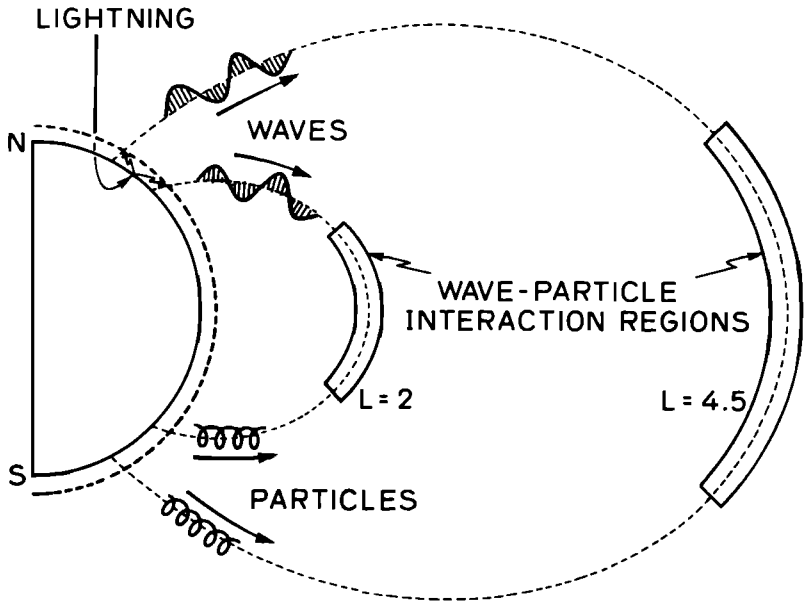

Fig. 1. Schematics showing the location of the lightning source and the wave-particle interaction regions.

distribution function and the time evolution of the precipitation flux.

2. Description of Models and Parameters

We consider the input energy source to be a lightning discharge that generates an impulsive electromagnetic wave that is assumed to enter the magnetosphere at 1000 km altitude at time t=0. The wave energy is assumed to propagate in a whistler "duct" along a field line so that the wave vector $\mathbf{k}$ can be taken as being parallel to the static magnetic field $\mathbf{B_0}$. The propagating whistler interacts with energetic electrons for which the resonance condition

$$2\pi f - \mathbf{k}\cdot\mathbf{v} \simeq 2\pi f_H/\gamma \qquad (1)$$

is locally satisfied, where f is the wave frequency, f_H is the local electron gyrofrequency, $\mathbf{v}$ is the total velocity of the electron, and $\gamma = (1 - v^2/c^2)^{-1/2}$ is the relativistic factor. For a whistler mode wave ($f_H > f$), (1) is satisfied for electrons that travel in a direction opposite to that of the wave (excluding the case of $f_H/\gamma < f$ which requires an impractically high particle pitch angle and is therefore not considered here).

Equatorial Cold Plasma Density Profile

We consider the interaction between a whistler wave and energetic electrons on field lines between L=2 and 4.5. Figure 1 gives a pictorial view of the wave-particle interaction. For the background magnetosphere we use a centered dipole model of the earth's magnetic field and a diffusive equilibrium model for the cold plasma distribution along the field lines. We choose an equatorial electron density defined by $N_{eq} = 8128/10^{0.359L}$ el cm^{-3}, as illustrated in Figure 2, which was found from whistler measurements to be an "average" plasmaspheric density distribution [*Park et al.*, 1978]. Also shown in Figure 2 is the value of the equatorial bounce

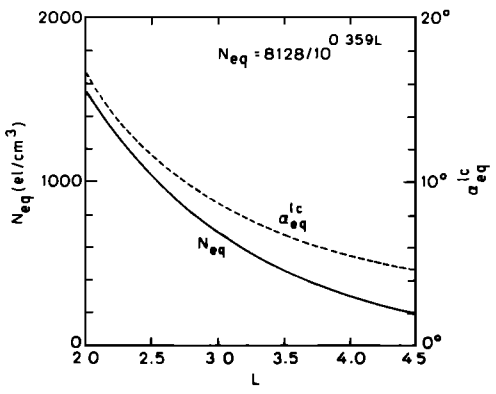

Fig. 2. The equatorial cold plasma density and the equatorial bounce loss cone used in the model calculation.

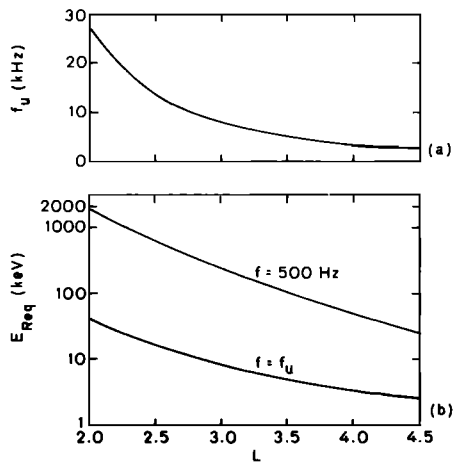

Fig. 3. (*a*) The upper frequency ($f_u = f_{Heq}/4$) of the simulated whistler as a function of L. (*b*) The equatorial resonance energy (E_{Req}) as a function of L corresponding to f_u and 500 Hz, respectively, based on the cold plasma density model described in Figure 2.

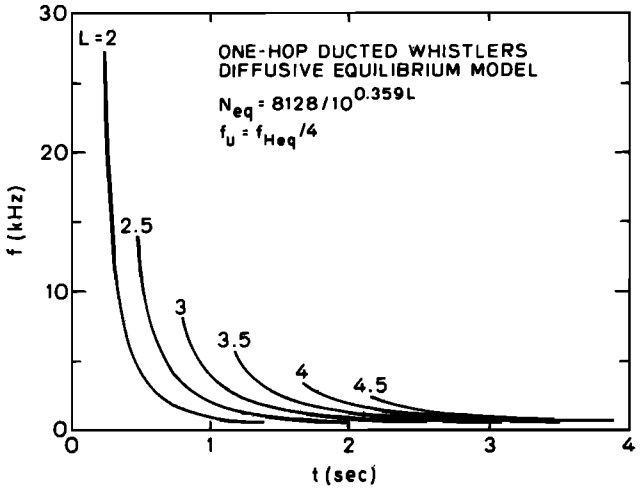

Fig. 4. The frequency-time formats over the frequency range of 500 Hz to f_u for one-hop whistlers propagating on L shells of 2 to 4.5. The lightning-generated wave impulse is injected at t=0 in the northern hemisphere.

loss cone as a function of L. The loss cone angles are derived from the dipole magnetic field model by using a mirror height of 100 km.

Whistler Frequency Range

We consider lightning flashes occurring in the northern hemisphere that launch VLF energy into different field-aligned ducts. The wave energy propagates southward and arrives at southern conjugate points as a one-hop whistler. For each L shell we consider the one-hop whistler with frequency components $f < f_u = f_{Heq}/4$, where f_{Heq} is the equatorial gyrofrequency. Figure 3 shows f_u versus L and the corresponding equatorial particle resonance energy E_{Req} based on a centered dipole model for the geomagnetic field, and the density model discussed above. For a variable frequency signal with upper cutoff frequency f_u, E_{Req} corresponding to this upper frequency represents the minimum particle energy for which gyroresonance can occur anywhere along a given field line.

The lower frequency of the whistlers is taken to be 500 Hz regardless of the L shell of propagation. Thus along each field line we assume a propagating whistler extending over the frequency range of f_u to 500 Hz. The equatorial resonance energy corresponding to 500 Hz is shown in Figure 3*b* as a function of L. Figure 4 shows idealized $f-t$ curves over the frequency range considered for one-hop whistlers at different L values, as they would be observed at the southern conjugate points after the injection of the impulse at t=0 in the northern hemisphere.

Wave Power Spectrum and Intensity

The power spectral density of the input wave impulse at each L is assumed to be identical and is taken to be proportional to $\exp\left[-(\log_{10}(f/5.0))^2/(0.4)^2\right]$, where f is the frequency in kilohertz. This represents a Gaussian distribution peaked at 5 kHz, which approximates the spectra of signals radiated by lightning obtained in various observations [*Pierce*, 1977]. In adopting this distribution we realize that the power spectral density distribution in individual events can be very different and that the assumed distribution represents an "average" case. Also, we neglect the change in the wave power spectrum that would inevitably occur due to such frequency dependent effects as absorption during propagation through the lower ionosphere and the coupling of the wave energy into a whistler duct. Once the wave packet is in the duct, the strength of the wave magnetic and electric fields of any frequency component at a given point along the field line depends on the local refractive index as well as the dispersion of the wave packet since the total propagating wave energy is conserved. These effects have been included here as well as in previous applications of the test particle model [*Chang et al.*, 1983] since they determine the wave parameters within the individual wave-particle interaction regions. Figure 5 shows the wave intensity at the equatorial plane at frequencies f_u and 1 kHz for different L shells. The absolute value of the product of the input wave power spectral density at 5 kHz and the temporal duration of the input impulse is taken to be 10^{-12} W m^{-2} Hz^{-1} s (or 10^{-12} m^{-2} Hz^{-1}), resulting in an equatorial wave magnetic field intensity of ~8 pT at L=3.5 and f=5.1 kHz, as shown in Figure 5.

Energetic Particle Distribution

The initial unperturbed distribution of energetic electrons is represented by an equatorial distribution function $f(E,\alpha)$, where E is the total energy and α is the equatorial pitch angle of the particle. We assume that $f(E,\alpha)$ is of the form [*Chang and Inan*, 1983*a*]

$$f(E,\alpha) = \Phi_{E_0}\left(\frac{m}{c^2}\right)\left(\frac{\gamma_0^5}{\gamma_0^2-1}\right)E_0^{n/2}E^{-n/2}g(\alpha) \quad (2)$$

for $\alpha \geq \alpha^{lc}$. In the above, Φ_{E_0} in el cm^{-2} s^{-1} sr^{-1} keV^{-1} is the differential energy spectral intensity of electrons at energy E_0(keV) and with $\alpha = 90°$ pitch angle, m is the rest mass of the electron, γ_0 is the relativistic factor associated with the energy E_0, $n/2$ is an exponent that determines the falloff in energy of the distribution, $g(\alpha)$ accounts for the anisotropy of the distribution, and α^{lc} is the angular half width of the loss cone. In this paper we consider an initially empty loss cone so that $f(E,\alpha) = 0$ for $\alpha < \alpha^{lc}$ and we assume that $g(\alpha) = 1$ for $\alpha \geq \alpha^{lc}$. We present our results normalized to Φ_{E_0} with Φ_{E_0} taken to be constant with L. For the general case of Φ_E varying with L, the precipitated flux can be obtained by proper scaling of the results, since the wave-induced flux is proportional to Φ_{E_0} [*Inan et al.*, 1982].

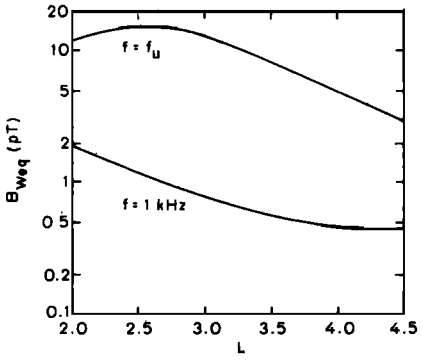

Fig. 5. The wave magnetic field intensities at the equatorial plane at frequencies f_u and 1 kHz as functions of L.

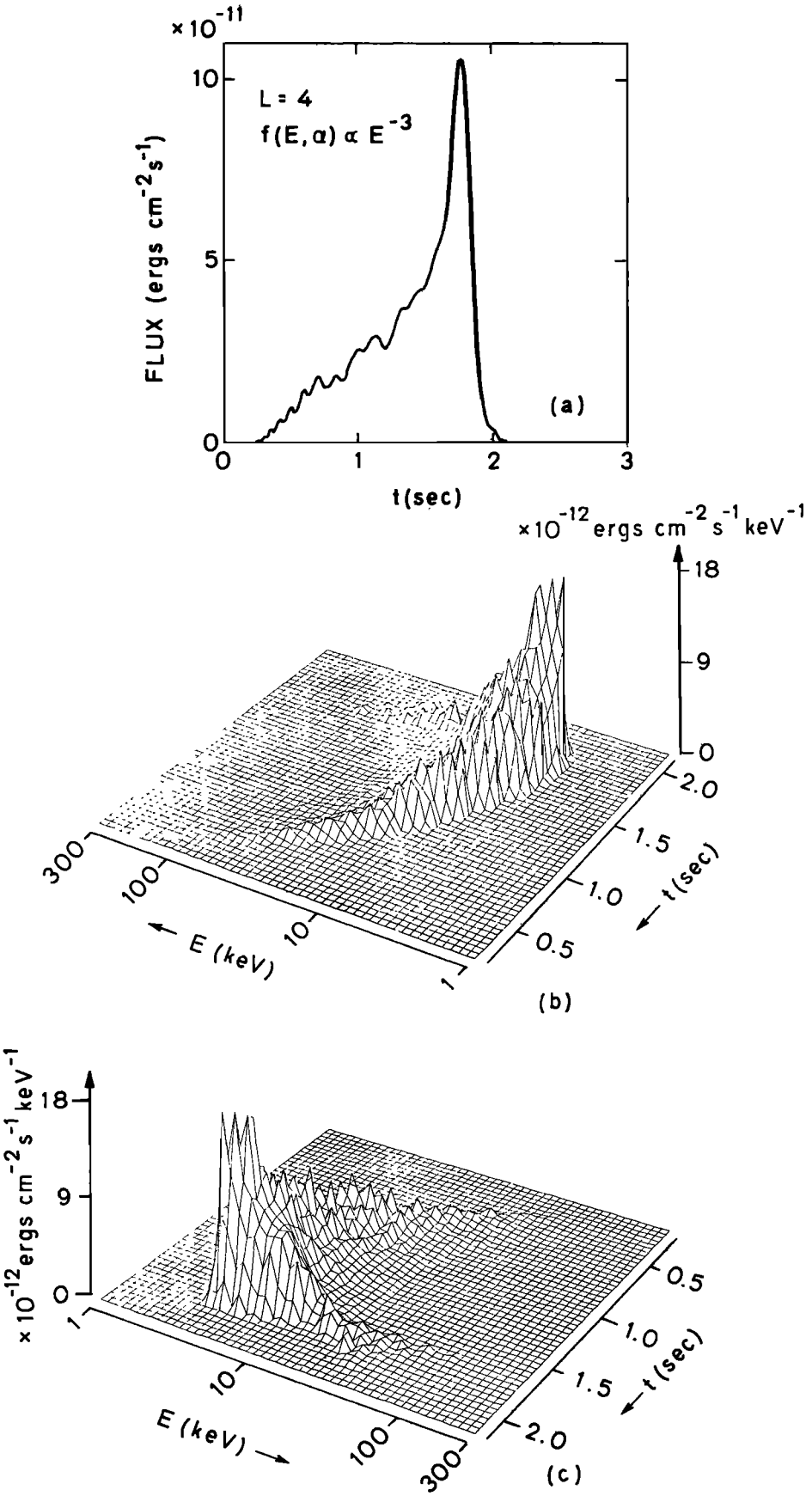

Fig. 6. (*a*) The computed precipitated energy flux versus time as would be observed in the northern hemisphere after the injection of the impulse wave energy at $t=0$ in the same hemisphere at $L=4$. (*b*) The evolution of the energy flux as a function of energy and time, representing the dynamic spectrum of the wave-induced flux shown in Figure 6*a*. (*c*) The same flux-energy-time diagram from a different perspective.

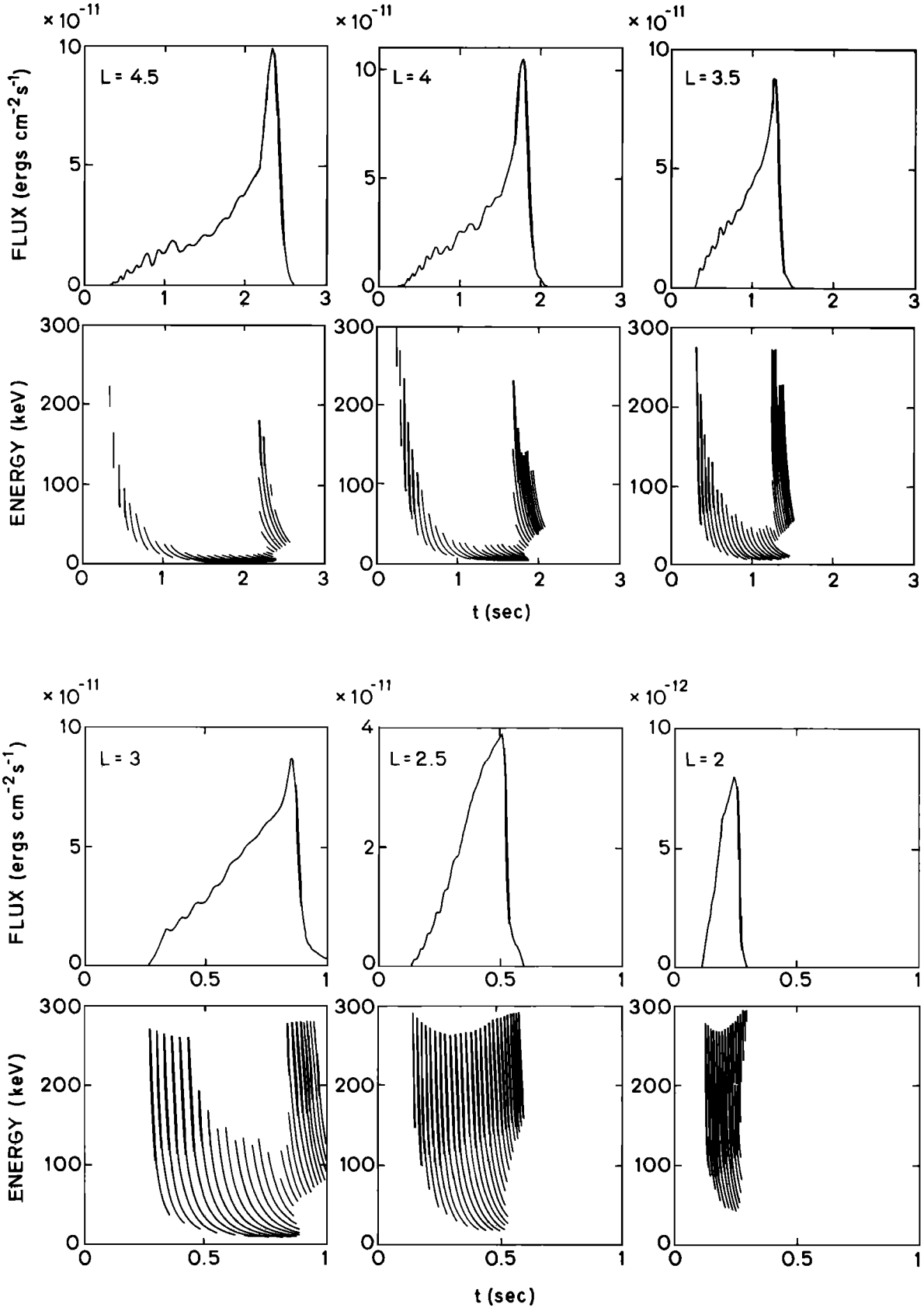

Fig. 7. Precipitated energy flux and the energy of particles constituting the flux plotted versus time for different L. The time scale for L=3 to 2 is different from that for L=4.5 to 3.5. These results were obtained by taking $\Phi_{E_0} = 1$ el cm^{-2} s^{-1} sr^{-1} keV^{-1} for E_0=1 keV and n=6 in equation (2).

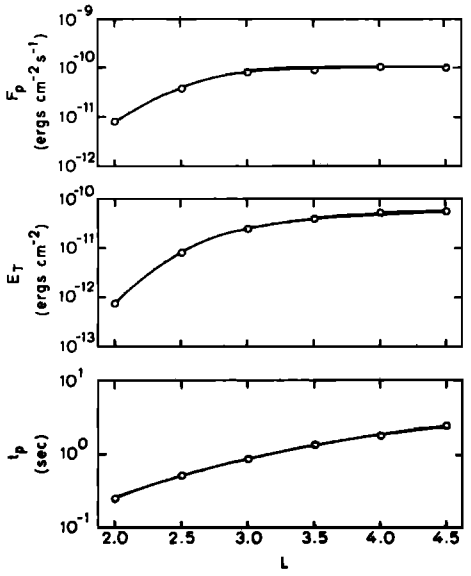

Fig. 8. Peak flux F_P, integrated energy deposition E_T, and the arrival time t_P of the peak as functions of L for the cases shown in Figure 7.

3. RESULTS

Time Evolution of Precipitated Flux

The precipitated energy fluxes are obtained by computing the trajectories of test particles from the distribution described by (2) and by integrating the downcoming electron flux over those particles scattered into the loss cone [*Inan et al.*, 1982]. Figure 6*a* shows the computed precipitated energy flux in ergs per square centimeter per second versus time as it would be observed in the northern hemisphere, where t=0 represents the initial position of the wave packet at 1000 km altitude in the northern hemisphere at L=4. For the case shown, we have taken $\Phi_{E_0} = 1$ el cm^{-2} s^{-1} sr^{-1} keV^{-1} for E_0=1 keV and n=6 in (2).

The result of Figure 6*a* represents the transient deposited energy flux integrated over particle energy. The pitch angle resolution of the calculation was chosen such that individual particles for which the equatorial pitch angle scattering $\Delta\alpha_{eq} < 0.01°$ were assumed to be unaffected by the wave. This criterion determines the upper limit of the energy of particles that would contribute to the estimated precipitated flux. In Figure 6*b* we present a three-dimensional flux-energy-time diagram, representing the "dynamic spectrum" of the wave-induced flux that would be observed in the northern hemisphere. Figure 6*c* shows the same function from a different perspective.

The energy content of the transient precipitation at different times during the wave-induced event can be followed from Figure 6*b* or 6*c*. As the wave packet propagates up the field line, it first resonates with higher-energy electrons at high northern latitudes; those electrons that are precipitated then arrive early at the lower ionosphere. The resonant energy gradually decreases as the wave approaches the geomagnetic equator and the precipitated flux increases due to the more efficient wave-induced pitch angle scattering and increased number of trapped particles (for the assumed $f(E,\alpha)$) near the equator. After the wave crosses the equator the upstream particles with successively higher energies interact with the wave, with the result that higher-energy electrons arrive at the wave injection site at the same time or even earlier than softer electrons which were scattered at earlier times. This arrival time "focusing" effect, seen near $t \simeq 2$ s in this case, was described in earlier work for monochromatic signals [*Helliwell et al.*, 1980; *Inan et al.*, 1982].

Results similar to that of Figure 6*a* are presented in Figure 7 for six different cases of L=4.5, 4.0, 3.5, 3.0, 2.5, and 2.0, based on the parameters described in the previous section and the same assumptions made in connection with Figure 6. For each case we present the flux versus time and a diagram demonstrating the progression of the range of the resonant energies as the wave propagates. These "energy curves" represent the range of contributing resonant particle energies when particles are considered to encounter the wave at a sequence of discrete wave front locations along the field line [*Inan et al.*, 1982]. Using the case of L=4 as an example, the left and right groups of curves represent, respectively, electrons which are scattered by the wave before and after it reaches the geomagnetic equator. Lower-energy electrons

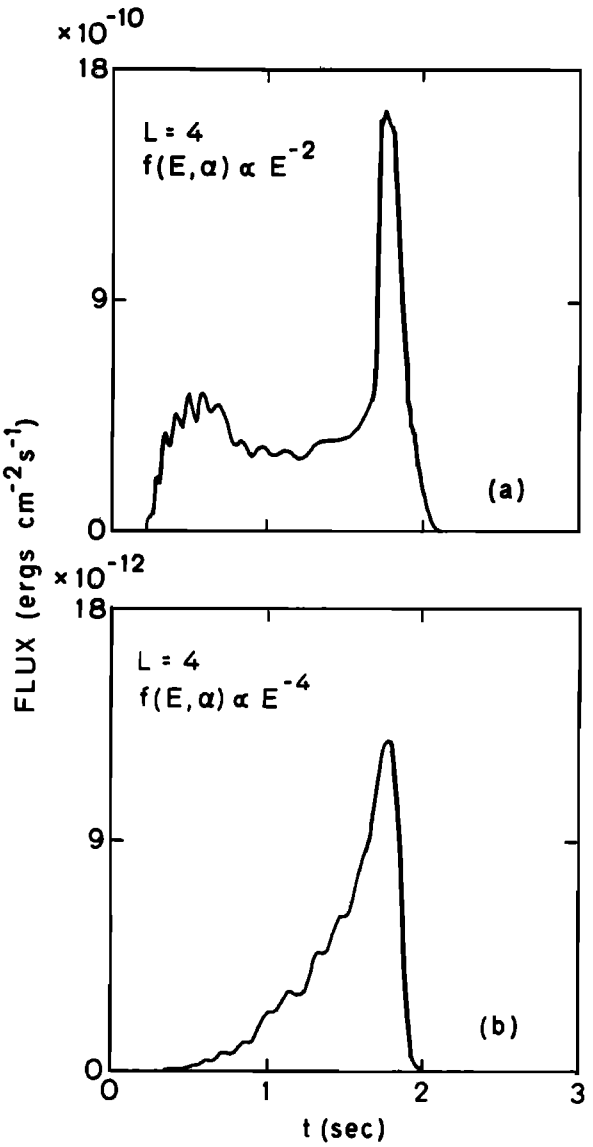

Fig. 9. Precipitated energy flux versus time for the case of L=4 for (*a*) n=4 and (*b*) n=8 in equation (2). All other parameters have the same value as in Figure 6.

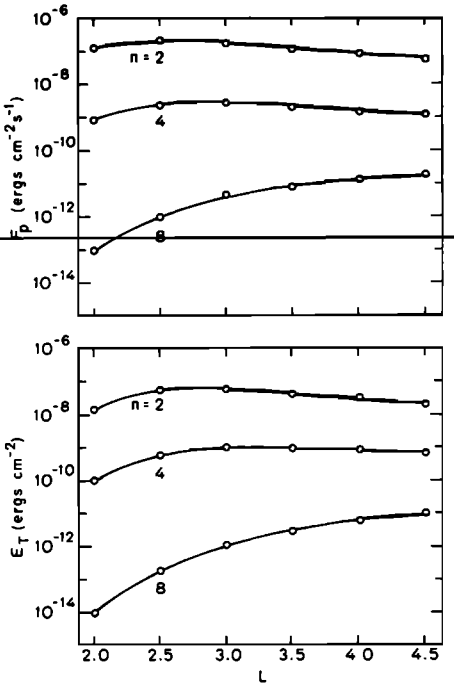

Fig. 10. Peak flux F_P and integrated energy deposition E_T as functions of L for n=2, 4, and 8. All other parameters have the same value as in Figure 8.

generally interact with the wave near the equator [*Chang and Inan*, 1983*b*].

We consider only those electrons with energy less than 300 keV, so that the energy curves for the case of L=2 are terminated at 300 keV. By comparing the peak of the transient precipitation pulse with the energy curves for each case, we see that the peak flux is due mainly to the arrival time focusing of the high- and low-energy electrons, as discussed above.

The duration of the precipitation pulse is principally determined by the wave and electron travel times along the given field line. In comparing the times of arrival of the electron pulses on different field lines, the faster arrival of the precipitation on lower L shells is mainly due to the shorter travel time of the whistler over the field line. In Figure 7 the time scale of the last three cases is reduced relative to that of the first three. Note that the flux scale in each case is also different. We have assumed the electron distribution represented by $\Phi(E,\alpha)$ to be the same on the various L shells. Figure 7 shows that the peak flux value increases as L increases, with that for L=4.5 being ~8 times larger than that for L=2. The peak flux F_P is plotted as a function of L in Figure 8. Also shown is the integrated energy deposition E_T (in ergs per square centimeter) obtained by integrating the transient precipitated energy flux over time and the arrival time t_P of the peak flux. The quantities F_P and E_T were previously shown to approximately characterize transient precipitation pulses [*Inan et al.*, 1982]. Both F_P and E_T increase with L, with E_T changing by a larger factor due to the longer duration of the precipitation pulse on higher L shells.

The Role of the Distribution Function

The results of Figures 6, 7, and 8 are for an energetic electron distribution function with n=6 in (2). As was shown previously [*Inan et al.*, 1982; *Chang et al.*, 1983], the temporal shape as well as the peak value of the precipitation pulse depends markedly on the spectral shape of the initial trapped distribution. To assess this effect for lightning-induced precipitation, in Figure 9 we show the time evolution of the precipitated flux for L=4 and for two different distributions with n=4 and 8 in (2). For each distribution Φ_{E_0} is assumed to be the same. As a result, for smaller n the downcoming flux is larger since more particles are available. Note that the flux scales for these two cases are different. The leading portion of the precipitation pulse is largely controlled by the energy dependence of the trapped distribution function, since it is composed of electrons of higher energy, as shown in Figure 7. (Note that the energy curves of Figure 7 are independent of n, since these only show the energy range of the downcoming particles that contribute to the flux at any given time, regardless of the relative amount of flux at the various energies.) The smaller flux level and the slower buildup of the leading edge of the electron pulse for the n=8 distribution compared with those of the n=4 case and the n=6 case shown in Figure 6*a* are attributed to the reduced number of available electrons in the high-energy range.

The L dependence of F_P and E_T for n=2, 4, and 8 are given in Figure 10. The differential energy spectral intensity Φ_{E_0} at E_0=1 keV is taken to be 1 el cm^{-2} s^{-1} sr^{-1} keV^{-1} for all cases. For n=2 and 4 the variation of the flux with L becomes smaller compared to that for n=8 and the case of n=6 shown in Figure 8. Note that for n=4 the computed fluxes are only different within a factor of 2 for L >2.5; the reduced efficiency in wave-induced pitch angle scattering for lower L is balanced by a wider range of higher-energy electrons that are scattered.

The Higher-Energy Precipitation Flux

Up to now we have considered precipitated energy flux consisting of electrons of energy from E_{Req} (corresponding to f_u) to 300 keV. Figure 11*a* shows the precipitated energy fluxes contributed by electrons with E >40 keV for L=4. The significance of precipitation due to higher-energy particles in connection with the resulting ionospheric perturbations is discussed in the next section. The precipitation above 40 keV consists of two pulses; a result that can be understood considering the energy curves of Figure 7. The first pulse represents those electrons scattered by the wave on the downstream side of the equator for the particles, while the second pulse is caused by wave-particle interactions on the upstream side.

Figure 11*b* shows the > 40 keV flux for L=2. Note that this is identical to that shown for the same L shell in Figure 7, since the minimum resonant energy for this L shell is > 40 keV, as shown in Figure 3.

Conjugacy of Whistler-Induced Precipitation

We have considered the fluxes that would be precipitated into the northern hemisphere for the case of lightning-induced wave energy injected into the magnetosphere in the north. Under the same excitation conditions, precipitation can also occur in the southern hemisphere because (1) a fraction of wave-scattered electrons can backscatter from the atmosphere in the northern hemisphere, with the fractional backscatter being as high as 80–90% depending on

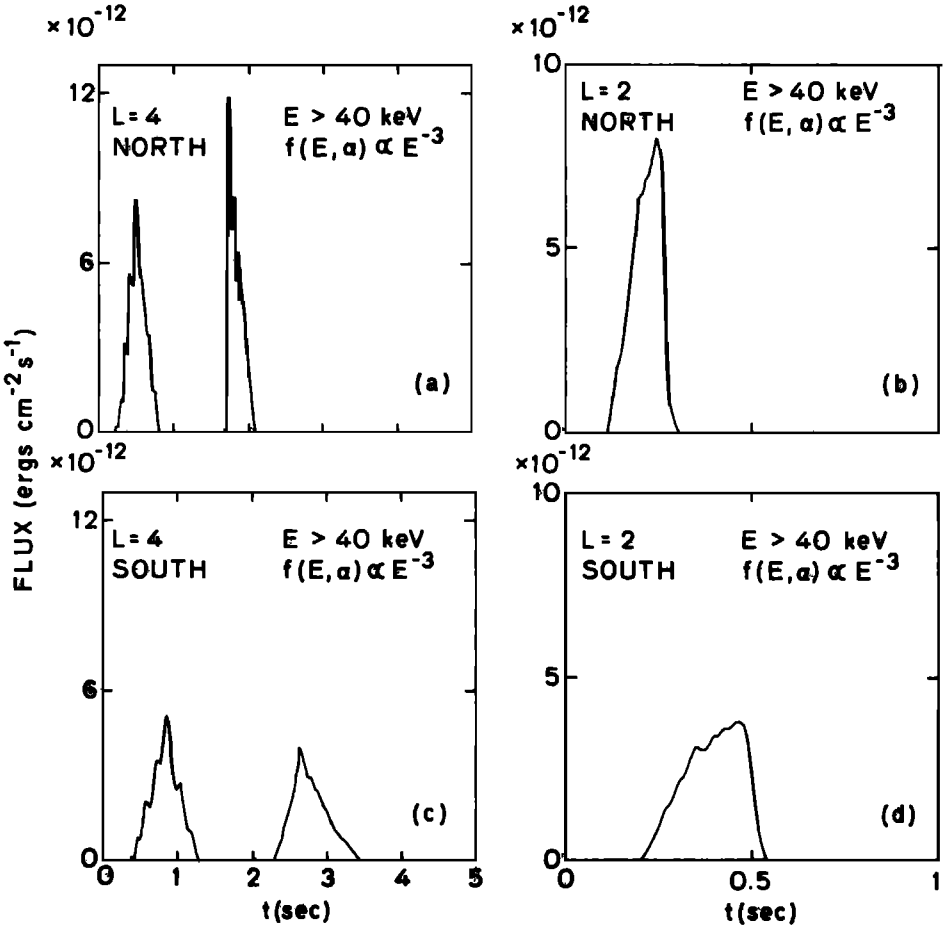

Fig. 11. (*a*),(*b*) The precipitated northern hemisphere energy fluxes versus time contributed by electrons with $E > 40$ keV at L=4 and 2. The same Φ_{E_0} and n as in Figure 7 were used. (*c*),(*d*) The mirrored precipitation fluxes that would be observed at the conjugate site in the southern hemisphere assuming that all the scattered electrons considered in Figures 11*a* and 11*b* mirror or backscatter in the north and precipitate in the south.

the particle's local pitch angle [*Stadsnes and Maehlum*, 1965; *Berger et al.*, 1974], and, (2) the mirror height of particles in the north could be higher than that in the south due to an asymmetry in the earth's magnetic field strength as would be the case at longitudes near the South Atlantic magnetic anomaly [*Barish and Wiley*, 1970].

As an example, on the Siple (76°S, 84°W)-Roberval field line a mirror height of 100 km in the south corresponds to a conjugate mirror height of 280 km, amounting to $\sim 0.2°$ difference in the half angle of the equatorial loss cone between the two hemispheres. Along field lines closer to the anomaly, for example, near Palmer, Antarctica (65°S, 64°W), where large numbers of whistler-induced precipitation events have been observed (see discussion section), the difference in equatorial loss cone half angles can be as high as 1–2°.

In Figures 11*c* and 11*d* we show the mirrored precipitation fluxes that would be observed at the conjugate site in the south. Here we assume that all the scattered electrons above 40 keV considered in Figures 11*a* and 11*b* mirror or backscatter in the north and precipitate in the south. Note that the mirrored precipitation pulses have longer durations than those for the direct precipitation (Figures 11*a* and 11*b*) as a result of the dispersion of electrons having different energies.

The conjugate flux can be due to mirror height asymmetry, atmospheric backscatter, or both. A phased sequence of northern and southern hemisphere fluxes due to the bounce motion of the whistler-scattered particle population may occur. If the pitch angle dependent atmospheric backscatter [*Berger et al.*, 1974; *Inan et al.*, 1985] is quantitatively accounted for, the flux observed at the northern or southern hemispheres would be a succession of pulse groups such as those shown in Figure 11, with successive pulse groups separated by a time representing a weighted average of the particle bounce times over the range of energies that constitute the flux. The intensity of the flux would progressively decrease due to fractional loss at hemispheric encounters and the pulse durations would be progressively wider due to energy dispersion. Note that the whistler wave durations (Figure 4) is typically shorter than the precipitation pulse so that such a succession of particle pulses may last well beyond the wave packet. A particle event such as the one described has been observed recently on a low-altitude satellite in one-to-one correlation with whistlers observed at a ground station near the conjugate region [*Voss et al.*, 1984].

Absolute Flux Level

The flux results presented in Figures 6–11 have been normalized to $\Phi_{E_0} = 1$ el cm^{-2} s^{-1} sr^{-1} keV^{-1} at E_0=1

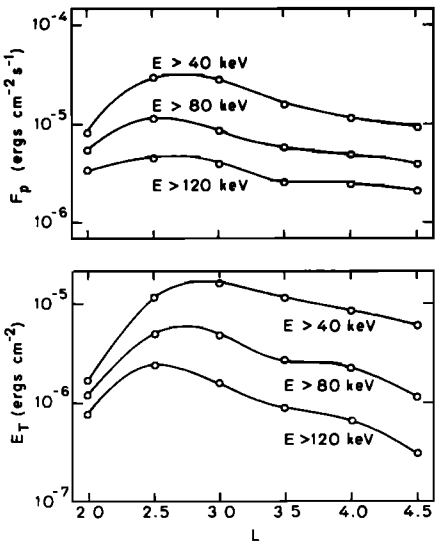

Fig. 12. Peak flux F_P and integrated energy deposition E_T as functions of L for the mirrored precipitation in the south for energies above 40, 80, and 120 keV. A trapped distribution with n=6, $g(90°)/g(\alpha^{lc}) \simeq 10$, and $\Phi_{E_0} = 10^4$ el cm^{-2} s^{-1} sr^{-1} keV^{-1} at 90° pitch angle for E_0=40 keV was assumed for different L.

keV. To estimate the order of magnitude of the absolute flux level, we consider a typical quiet time value for Φ_{E_0} of $\Phi_{E_0} \simeq 10^4$ el cm^{-2} s^{-1} sr^{-1} keV^{-1} at 90° pitch angle and $g(90°)/g(\alpha^{lc}) \simeq 10$ for E_0=40 keV and at $L \simeq 4$ [*Lyons and Williams*, 1975]. This gives a peak flux of 1.1×10^{-5} ergs cm^{-2} s^{-1} for the mirrored precipitation shown in Figure 11*c* for the case of L=4.

It should be noted here that the absolute level of the precipitation flux is dependent (nearly proportional) to the assumed equatorial wave magnetic field intensity $B_{W\text{eq}}$. The fluxes presented so far were for a lightning-generated wave packet having a Gaussian spectral density distribution with peak value of 10^{-12} cm^{-2} Hz^{-1} at 5 kHz, resulting in the L dependent equatorial wave magnetic field intensity distribution shown in Figure 5. This shows $B_{W\text{eq}}$ of 3–15 pT for $f=f_u$.

While such a value is within the range of whistler intensities as observed in situ on satellites, it does not necessarily represent a typical wave signal level for whistlers. A statistical analysis of satellite-observed whistler intensities is yet to be carried out. However, recent Stanford University experiments on the Dynamics Explorer 1 satellite show that wave magnetic field intensities in the approximate range of 0.1–100 pT are at least occassionally observed. In any case, our use of a peak energy spectral density of 10^{-12} m^{-2} Hz^{-1} is merely based on an attempt to achieve a convenient means of normalization that also results in an equatorial wave intensity that is at least occasionally observed. Signal levels during individual cases can be different; however, the resulting precipitation fluxes can be estimated using our results by proper scaling, since the flux is to first-order proportional to $B_{W\text{eq}}$ [*Inan et al.*, 1982].

4. Discussion: Implications for the "Trimpi" Phenomenon

The higher-energy component of the precipitated particle flux is particularly relevant to the detection of the ionospheric effects of such precipitation and to the "Trimpi" phenomenon discussed in the introduction. In order to be able to perturb subionospheric signal propagation, the precipitation must be of sufficient energy to penetrate below the ionospheric reflection height for VLF/LF signals. Perturbations at or below the D region (80–90 km) are possible for electron energies greater than 40 keV [*Banks et al.*, 1974].

In view of this, we present in Figure 12 the L variations of the peak and integrated energy flux (F_P and E_T) constituted by higher-energy electrons in selected ranges (i.e., E > 40, 80, and 120 keV), computed using n=6 in (2) and the above-mentioned typical quiet time value for Φ_{E_0} ($\simeq 10^4$ el cm^{-2} s^{-1} sr^{-1} keV^{-1}), assumed to be constant as a function of L. The results indicate that for these energy ranges the whistler-induced precipitation flux at $L < 3$ can be as large or larger than that at higher L shells. This result is to some degree dependent on the assumed cold plasma distribution, since this determines the gyroresonant electron energy along the field lines. Note that the equatorial resonant energies corresponding to the lowest (500 Hz) and highest (f_u) frequencies of the whistlers considered are shown in Figure 3*b*. As an example, 40 keV electrons do not resonate at the equator with the whistlers considered on $L > 4$. However, resonant interactions do occur off the equator, and this accounts for the precipitated fluxes shown in Figures 11 and 12. The results of Figure 12 quantitatively show that equatorial interactions at lower L shells are roughly as efficient in terms of wave-induced scattering as off-equatorial interactions on higher L shells.

The results of Figure 12 are for a constant Φ_{E_0} versus L. We now consider a typical observed quiet time L dependence of Φ_{E_0} for E_0=40 keV at 90° pitch angle [*Lyons and Williams*, 1975], as shown in the top panel of Figure 13. The L dependence of the estimated peak and integrated energy fluxes for E > 40 keV obtained by scaling this profile are shown, respectively, in the middle and lower panels of Figure 13. We have assumed an anisotropic pitch angle distribution with $g(90°)/g(\alpha^{lc}) \simeq 10$ for all L shells. The result suggests that under quiet time conditions, the region of $L < 3$ is even

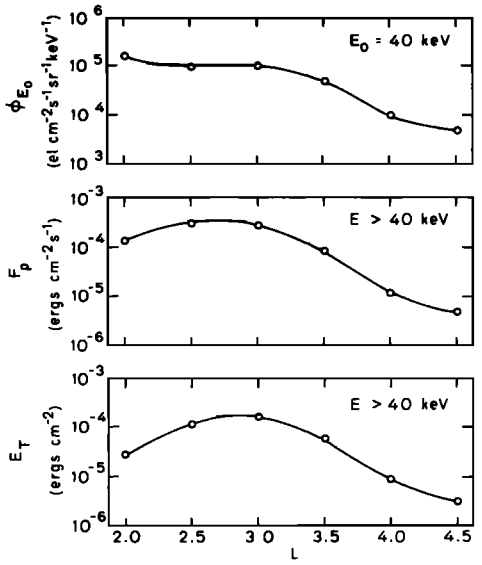

Fig. 13. Results obtained by scaling F_P and E_T for the case of E > 40 keV in Figure 12 using a variation of Φ_{E_0} as a function of L shown in the top panel.

further favored as far as the whistler-induced precipitation of particles > 40 keV is concerned.

The above theoretical findings are generally consistent with observations of "Trimpi" events at Palmer, Antarctica [*Carpenter and LaBelle,* 1982; *Leyser et al.,* 1984], where occurrence rates of lightning-induced burst precipitation at $\sim 2 < L < 2.4$ were found to be at least as high as those reported earlier from higher latitudes [*Helliwell et al.,* 1973]. A low-latitude burst precipitation zone ($2< L <3$) was experimentally identified by *Doherty* [1971], although an association of the observed subionospheric perturbations with individual whistlers was not recognized at the time. Preliminary analysis of recent data from Palmer ($L \simeq 2.3$) and Siple ($L \simeq 4.3$), Antarctica, stations also suggests the existence of a preferred precipitation zone over L shells $\sim 2 < L <\sim 3.5$ (D. L. Carpenter, private communication, 1984). It should be emphasized, however, that a lot more experimental work is needed on statistical comparisons of activity at lower and higher L shells. Also, we note that "Trimpi" events tend to occur during and immediately following magnetic disturbances, when the Φ_{E_0} versus L might be different from that during quiet times. However, events are also seen to occur during quiet times [*Leyser et al.,* 1984], and in such cases the results of Figure 13 can be applied with more confidence.

5. Summary and Conclusions

In the context of an average model of the magnetospheric cold plasma density inside the plasmasphere [*Park et al.,* 1978], we have quantitatively estimated the time profile and energy spectra of precipitation fluxes that would be induced by lightning-generated whistlers at frequencies above 500 Hz and propagating on L shells of 2–4.5. The results presented can be used to interpret quantitatively observations of lightning-induced precipitation in terms of the time delay between whistler wave and particle fluxes and in terms of the energy spectrum of precipitation that can be observed by satellite or rocket based particle counters or X ray detectors.

Although our calculations were carried out for a specific "average" plasmaspheric cold plasma density profile, the results should be useful in assessing the L dependence of whistler-induced precipitation in the magnetosphere. By proper scaling, the results given can be used to estimate the magnitude of expected fluxes for various particle distributions when the trapped flux level Φ_{E_0} and the equatorial wave intensity $B_{W_{eq}}$ can be measured or estimated.

When only the high-energy electrons ($E > 40$ keV) are considered, our results indicate that whistler-induced precipitation at lower latitudes ($L < 3$) can be expected to be at least as high as that at higher latitudes. In fact, quantitative estimates identify an inner magnetospheric region ($2 < L <3$) where whistler-induced precipitation is expected to be relatively high. This finding is in general agreement with recent experimental findings and may be important in the context of experiments aimed at detecting lightning-induced precipitation at mid-to-low latitudes, such as the measurement of subionospheric VLF/LF signal perturbations caused by precipitation-induced density enhancements in the ionospheric D region.

Acknowledgments. We acknowledge many discussions with our colleages in the STAR Laboratory. This work was supported by the National Aeronautics and Space Administration under grant NGL-05-020-008. The work of one of us (H. C. C.) was also partly supported by the Fleischmann Foundation.

The Editor thanks Bruce Edgar for his assistance in evaluating the above paper.

References

Banks, P. M., C. R. Chappell, and A. F. Nagy, A new model for the interaction of auroral electrons with the atmosphere: Spectral degradation, backscatter, optical emission, and ionization, *J. Geophys. Res., 79,* 1495, 1974.

Barish, F. D., and R. E. Wiley, World contours of conjugate mirror locations, *J. Geophys. Res., 75,* 6342, 1970.

Berger, M. J., S. M. Seltzer, and K. Maeda, Some new results on electron transport in the atmosphere, *J. Atmos. Terr. Phys., 36,* 591, 1974.

Carpenter, D. L., and J. W. LaBelle, A study of whistlers correlated with bursts of electron precipitation near L=2, *J. Geophys. Res., 87,* 4427, 1982.

Carpenter, D. L., U. S. Inan, M. L. Trimpi, R. A. Helliwell, and J. P. Katsufrakis, Perturbations of subionospheric LF and MF signals due to whistler-induced electron precipitation bursts, *J. Geophys. Res., 89,* 9857, 1984.

Chang, H. C., and U. S. Inan, Quasi-relativistic electron precipitation due to interactions with coherent VLF waves in the magnetosphere, *J. Geophys. Res., 88,* 318, 1983*a*.

Chang, H. C., and U. S. Inan, A theoretical model study of observed correlations between whistler mode waves and energetic electron precipitation events in the magnetosphere, *J. Geophys. Res., 88,* 10,053, 1983*b*.

Chang, H. C., U. S. Inan, and T. F. Bell, Energetic electron precipitation due to gyroresonant interactions in the magnetosphere involving coherent VLF waves with slowly varying frequency, *J. Geophys. Res., 88,* 7037, 1983.

Cornwall, J. M., Scattering of energetic trapped electrons by very-low-frequency waves, *J. Geophys. Res., 69,* 1251, 1964.

Doherty, R. H., Observations suggesting particle precipitation at latitudes below 40°N, *Radio Sci., 6,* 639, 1971.

Doolittle, J. H., and D. L. Carpenter, Photometric evidence of electron precipitation induced by first hop whistlers, *Geophys. Res. Lett., 10,* 611, 1983.

Dungey, J. W., Loss of Van Allen electrons due to whistlers, *Planet. Space Sci., 11,* 591, 1963.

Helliwell, R. A., *Whistlers and Related Ionospheric Phenomena,* Stanford University Press, Stanford, Calif., 1965.

Helliwell, R. A., J. P. Katsufrakis, and M. L. Trimpi, Whistler-induced amplitude perturbation in VLF propagation, *J. Geophys. Res., 78,* 4679, 1973.

Helliwell, R. A., S. B. Mende, J. H. Doolittle, W. C. Armstrong, and D. L. Carpenter, Correlations between λ4278 optical emissions and VLF wave events observed at $L \sim 4$ in the Antarctic, *J. Geophys. Res., 85,* 3376, 1980.

Inan, U. S., T. F. Bell, and H. C. Chang, Particle precipitation induced by short-duration VLF waves in the magnetosphere, *J. Geophys. Res., 87,* 6243, 1982.

Inan, U. S., H. C. Chang, R. A. Helliwell, W. L. Imhof, J. B. Reagan, and M. Walt, Precipitation of radiation belt electrons by man-made waves: A comparison between theory and measurement, *J. Geophys. Res.,* in press, 1985.

Leyser, T. B., U. S. Inan, D. L. Carpenter, and M. L. Trimpi, Diurnal variation of burst precipitation effects on subionospheric VLF/LF signal propagation near L=2, *J. Geophys. Res., 89,* 9139, 1984.

Lyons, L. R., and D. J. Williams, The quiet time structure of energetic (35-560 keV) radiation belt electrons, *J. Geophys. Res., 80,* 943, 1975.

Lyons, L. R., R. M. Thorne, and C. F. Kennel, Pitch-angle diffusion of radiation belt electrons within the plasmasphere, *J. Geophys. Res., 77,* 3455, 1972.

Park, C. G., D. L. Carpenter, and D. B. Wiggin, Electron density in the plasmasphere: Whistler data on solar cycle, annual, and diurnal variations, *J. Geophys. Res., 83,* 3137, 1978.

Pierce, E. T., Atmospherics and radio noise, in *Lightning,* vol. 1, *Physics of Lightning,* edited by R. H. Golde, Academic, Orlando, Fla., 1977.

Rosenberg, T. J., R. A. Helliwell, and J. P. Katsufrakis, Electron precipitation associated with discrete very-low-frequency emissions, *J. Geophys. Res., 76,* 8445, 1971.

Rycroft, M. J., Enhanced energetic electron intensities at 100 km altitude and a whistler propagating through the plasmasphere, *J. Planet. Space Sci., 21,* 239, 1973.

Stadsnes, J., and B. Maehlum, Scattering and absorption of fast electrons in the upper atmosphere, internal report, Norw. Def. Res. Estab., Kjeller, Norway, 1965.

Voss, H. D., W. L. Imhof, J. Mobilia, E. E. Gaines, M. Walt, U. S. Inan, R. A. Helliwell, D. L. Carpenter, J. P. Katsufrakis, and H. C. Chang, Lightning induced electron precipitation, *Nature,* in press, 1984.

H. C. Chang , Department of Electrical Engineering, National Taiwan University, Taipei, Taiwan, Republic of China.

U. S. Inan, Space, Telecommunications and Radioscience Laboratory, Stanford University, Stanford, CA 94305.

(Received August 3, 1984;
accepted September 26, 1984.)